

Visualizing Excitation Waves inside Cardiac Muscle Using Transillumination

William T. Baxter, Sergey F. Mironov, Alexey V. Zaitsev, José Jalife, and Arkady M. Pertsov

Department of Pharmacology, SUNY Health Science Center, Syracuse, New York 13210 USA

ABSTRACT Voltage-sensitive fluorescent dyes have become powerful tools for the visualization of excitation propagation in the heart. However, until recently they were used exclusively for surface recordings. Here we demonstrate the possibility of visualizing the electrical activity from inside cardiac muscle via fluorescence measurements in the transillumination mode (in which the light source and photodetector are on opposite sides of the preparation). This mode enables the detection of light escaping from layers deep within the tissue. Experiments were conducted in perfused (8 mm thick) slabs of sheep right ventricular wall stained with the voltage-sensitive dye di-4-ANEPPS. Although the amplitude and signal-to-noise ratio recorded in the transillumination mode were significantly smaller than those recorded in the epi-illumination mode, they were sufficient to reliably determine the activation sequence. Penetration depths (spatial decay constants) derived from measurements of light attenuation in cardiac muscle were 0.8 mm for excitation (520 ± 30 nm) and 1.3 mm for emission wavelengths (640 ± 50 nm). Estimates of emitted fluorescence based on these attenuation values in 8-mm-thick tissue suggest that 90% of the transillumination signal originates from a 4-mm-thick layer near the illuminated surface. A 69% fraction of the recorded signal originates from ≥ 1 mm below the surface. Transillumination recordings may be combined with endocardial and epicardial surface recordings to obtain information about three-dimensional propagation in the thickness of the myocardial wall. We show an example in which transillumination reveals an intramural reentry, undetectable in surface recordings.

INTRODUCTION

Optical mapping has been used to study electrical activity in a variety of cardiac tissues, including cell cultures (Rohr and Salzberg, 1994), thin tissue slices (Pertsov et al., 1993), isolated whole hearts (Salama et al., 1987; Girouard et al., 1996; Wikswo et al., 1995), and most recently, in vivo (Dillon et al., 1998). Various technologies have been used to simultaneously record from multiple sites, including arrays of photodiodes (Rohr and Salzberg, 1994; Girouard et al., 1996), laser scanning (Dillon et al., 1998), and CCD cameras (Pertsov et al., 1993; Wikswo et al., 1995; Witkowski et al., 1998). In tissue and whole heart experiments, optical mapping is usually conducted in an epi-illumination mode, in which the light source and photodetector are aimed at the same surface. In this mode, changes in transmembrane potential are detected from a thin (300–500 μm) layer of cells at the surface (Knisley, 1995; Girouard et al., 1996), constituting only a small portion of ventricular wall. However, heart tissue is three-dimensional: human ventricles may be over 1 cm thick. The three-dimensional propagation of electrical activity inside the ventricular wall during normal cardiac function, and particularly during arrhythmias,

has traditionally been studied using multiple plunge electrodes inserted into the heart wall (Pogwizd and Corr, 1987; Frazier et al., 1989; El-Sherif et al., 1997).

Here we describe extending standard cardiac optical mapping techniques to analyze intramural activation via the transilluminated fluorescent signal, in which the light is placed behind the tissue and fluorescence emitted from the opposite side is collected. Preliminary experiments in our laboratory using left ventricles of Langendorff-perfused rabbit hearts (5–10 mm thick) with a light source inserted in the ventricular cavity indicated that fluorescent light escaping from layers deep within ventricular tissue could be detected by the CCD camera system (Pertsov et al., 1994). In this paper we present a more rigorous pursuit of this approach using a more geometrically regular preparation: rectangular slabs of tissue from sheep right ventricles (8 mm thick). The main objectives of this study were 1) to characterize the transillumination signals and compare them with conventional epifluorescence recordings during simple transmural pacing; 2) to estimate the weighting functions for transillumination and epifluorescence signals based on measurements of light attenuation in the tissue at the excitation and emission wavelengths; 3) to calculate transillumination and epifluorescence signals during transmural propagation in a realistic model of the cardiac action potential with the experimentally measured weighting functions and to compare them with the experimental data; and 4) to compare transilluminated and epi-illuminated signals during more complex propagation; in this case, an episode of sustained ventricular tachycardia. Some of these results have been previously presented in preliminary form (Baxter et al., 1997a).

Received for publication 29 November 1999 and in final form 6 October 2000.

Address reprint requests to Jose Jalife, M.D., Professor and Chairman of Pharmacology, SUNY Upstate Medical University, 766 Irving Ave., Syracuse, NY 13210. Tel.: 315-464-7949; Fax: 315-464-8000; E-mail: jalifej@upstate.edu.

This work was supported in part by Grant HL39707 from the National Heart and Blood Institute.

© 2001 by the Biophysical Society
0006-3495/01/01/516/15 \$2.00

MATERIALS AND METHODS

Experimental preparation

Experiments were conducted in isolated coronary perfused slabs of the right ventricle. Hearts were rapidly removed from young sheep anesthetized with sodium pentobarbital (35 mg/kg i.v.) and flushed with cold cardioplegic solution (in mmol/l: glucose 280, KCl 13.44, NaHCO₃ 12.6, mannitol 34, at 4°C). The free ventricular wall was excised and a branch of the right coronary artery was cannulated and perfused with Tyrode's solution (in mmol/l: NaCl 130, KCl 4.0, CaCl₂ 1.8, MgCl₂ 1.0, NaHCO₃ 24, NaH₂PO₄ 1.2, glucose 5.6) at a pressure head of 80 mmHg. The solution was bubbled with a gas mixture of 95% oxygen and 5% CO₂; the pH was 7.4. Preparations had relatively smooth endocardial surfaces, avoiding the papillary muscle and any large trabeculations. The perfused area (2 × 2 cm², 8 mm thick at the center) was cut out, and its edges were sutured to a rectangular frame and placed in a superfusion chamber with ECG recording electrodes. The slabs were suspended vertically in the chamber with CCD cameras aimed at both the inner (endocardial) and outer (epicardial) surfaces. Both the perfusate and chamber solution were maintained at 37°C. The tissue was stimulated at 500 ms BCL (basic cycle length) by a point electrode. After a 30–40-min period of equilibration, an electromechanical uncoupler (diacetyl monoxime, 10 mM) was added to the perfusate to abolish contraction. The potentiometric dye di-4-ANEPPS (15 μg/ml) was administered via the perfusate at the beginning of the experiment. Several preparations were cut down the middle and illuminated along the cut transmural edge; the resulting fluorescence was uniform across the width of the tissue, indicating that dye was uniformly distributed to all depths of the tissue.

The perfusate was not recirculated for the duration of the experiments, which lasted 2–3 h. During perfusion, the preparations were stable and exhibited normal action potential characteristics (e.g., action potential duration and conduction velocity). The episode of monomorphic tachycardia shown in Fig. 9 was initiated by rapid pacing, after decreasing the temperature of both the perfusate and chamber solution to 28°.

The CCD optical mapping system

Optical mapping of electrical activity was carried out with a dual CCD camera system. Details of the video camera recording system have been previously published (Pertsov et al., 1993; Baxter et al., 1997b). The entire system was duplicated to enable simultaneous recordings from two cameras aimed at opposite surfaces of the isolated ventricular slab. Each system included a 250 W tungsten-halogen light source, excitation (520 ± 30 nm) and emission (640 ± 50 nm) filters, dichroic mirror (580 nm), video camera (model 6510, Cohu, Inc., San Diego, CA; 739 × 480 pixels), and 8-bit frame grabber (model 12, Epix, Inc., Buffalo Grove, IL). The frame intervals of both cameras, as well as the recording and stimulating electrode signals, were synchronized to a single master trigger. Pacing trials were acquired at 240 fps (4.17 ms frame intervals), with image size 168 × 60 pixels, and field of view 24 × 17 mm (0.14 mm/pixel horizontal resolution, 0.28 mm/pixel vertical resolution). The magnification factor was 0.06. The arrhythmia example was acquired at 120 fps (8.33 ms interval), with image size 280 × 114 pixels, field size 22 × 18 mm, horizontal resolution of 0.08 mm/pixel, and magnification factor 0.11. Each camera was equipped with a TV zoom lens ($f = 12.5\text{--}75$ mm, F/1.8, Javelin) with numerical aperture 0.28. With the lens focused on the side of the slab facing the camera, millimeter scale bars at both the near and far (8 mm beyond the focal plane) surfaces of the slab were in focus, within the range of magnifications used. Tissues were illuminated with a collimated beam, giving a uniform circular spot of light, ~2 cm in diameter.

A background image of quiescent tissue was subtracted from each frame of the movie to visualize the voltage-dependent signal. Spatial filtering by weighted averaging of neighboring pixels was carried out by convolution with cone-shaped rotationally symmetric kernels, after stretching the con-

trast of the image to fill all 8 bits (Pertsov et al., 1993). Cone filters of width 11 and 15 pixels were used for epi-illuminated and transilluminated data, respectively. The effective resolutions (spatial resolution (mm/pixel) × kernel width at half-height) were 0.84 and 1.12 mm, respectively, for epi-illuminated and transilluminated pacing data, and 0.48 and 0.64 mm for epi-illuminated and transilluminated data in the arrhythmia example. In addition, a temporal median filter (Witkowski et al., 1998) of length = 9 frames was applied to transilluminated data. The SNR of a region was calculated over time for each pixel, then averaged. SNR was computed as S/N_{RMS} , where S is the mean number of gray levels at the peak of the action potentials and N_{RMS} is the root-mean-square of the baseline during periods between activations (Fast and Kleber, 1993; Girouard et al., 1996; Baxter et al., 1997b).

Activation times of optical signals were defined as the 50% level between the maximum of the action potential and the minimum of the immediately preceding baseline points, interpolated between the two nearest frames. Isochrone maps were created by rounding the activation time at each point to the nearest desired interval spacing (2 ms for Fig. 3) or to the nearest frame (8.3 ms for Fig. 9).

Optical recording protocol

Optical recordings of both epi-fluorescence from the surface and transilluminated fluorescence were obtained by the two cameras simultaneously, first with one light source on, then with the other. Fig. 1 A schematically depicts the ventricular slab in transmural cross section with cameras viewing the endocardial and epicardial surfaces, and light source 1 illuminating the endocardial surface. While camera 1 recorded epi-fluorescence from the endocardial surface (endocardial movie), camera 2 recorded fluorescence transmitted through the tissue (referred to as TRANS1, the transilluminated recording from light source 1). The first light source was then shuttered and the epicardial side was illuminated with light source 2 for two more recordings (Fig. 1 B), this time from the epicardial surface (camera 2) and transillumination (camera 1), called the epicardial and TRANS2 movies, respectively. To ensure that the activation patterns did not change over the course of recordings, immediately after these acquisitions, additional epicardial and endocardial surface recordings were obtained with both lights on. The three sets of movies were obtained in under 2 min. The activation sequence was considered unchanged if the respective surface activation maps and the ECG remained unchanged throughout. Similarity was assessed by superimposing isochrone maps of the corresponding surface recordings. For stable arrhythmias, such as the example in Fig. 9, an additional set of control surface recordings was acquired before transillumination; the four sets of movies were obtained in ~4 min. Temporal registration was achieved by synchronizing the surface movie acquired simultaneously with each transilluminated movie with the corresponding surface movie acquired with both lights on.

Measurement of light penetration

Light attenuation was measured in ventricular slab preparations cut through the center of the perfused area, exposing the cut transmural edge, and placed back in the superfusion chamber. The perfused slab was irradiated with either the excitation or emission wavelengths, while a video camera aimed at a perpendicular side viewed the decay of light with tissue depth (resolution 40 pixels/mm). There was no fluorescent dye in the tissue. To create an average light decay profile for any given image, each row of pixels was shifted such that points at equivalent depths from the illuminated surface were vertically aligned. Each row was normalized by contrast stretching to 256 levels. All rows were then averaged together. Exponential decay functions were fit to the attenuation profiles away from the tissue surface; the decay constants of these fits were the penetration depths δ_{ex} and δ_{e} (in mm) for excitation and emission wavelengths, respectively. The slabs were rotated in order to assess the effect of myocardial structure on

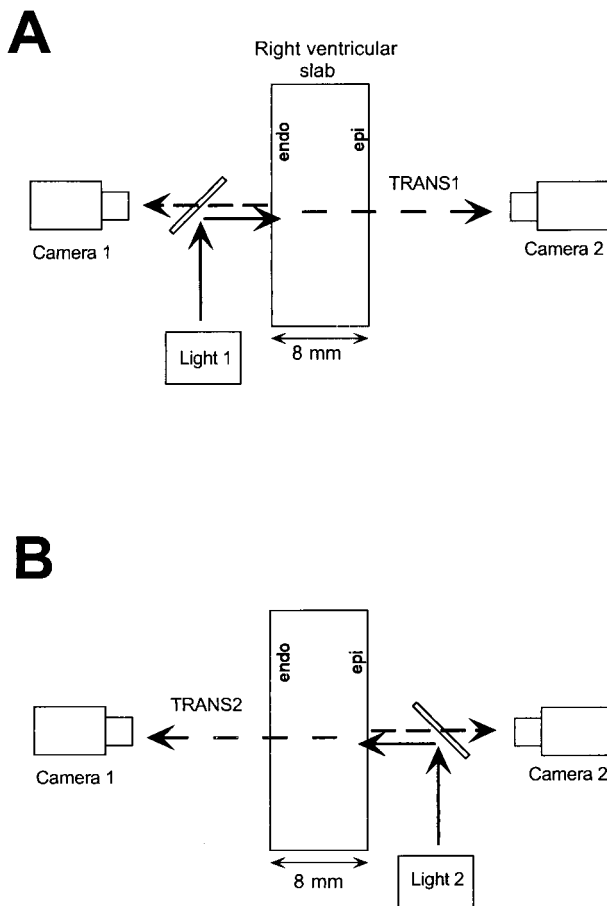


FIGURE 1 Schematic of optical recording system. The ventricular slab is suspended between two cameras and two light sources. (A) When light 1 is on, camera 1 records epifluorescence from the endocardial surface and camera 2 records fluorescence transmitted through the tissue. (B) Using light 2, camera 2 records from the epicardial surface and camera 1 records transilluminated fluorescence.

light attenuation: illumination was then on the transmural edge while light decay along the epicardial or endocardial side was viewed. A total of 12 decay profiles were obtained from 3 hearts (2 slabs each): 6 transmural, 3 epicardial, 3 endocardial. The decay constants were compared pairwise (i.e., epicardial versus transmural, endocardial versus transmural, epicardial versus endocardial) using a two-population *t*-test at the 0.05 significance level.

Measurements of light transmission were made with a lux meter (38039, Edmund Scientific, Barrington, NJ). Excitation light was measured with the meter at the tissue surface after the light had passed through filters and optics. Emitted fluorescence was measured with the meter at the position of the camera CCD after light had passed through the dichroic mirror, emission filter, and camera lens. Readings were corrected for area of the illuminated spot and the wavelength sensitivity of the meter. Lux were converted to radiometric units using the conversion $1 \text{ lux} = 2.062 \text{ mW/m}^2$ and 8.366 mW/m^2 at 520 nm and 640 nm, respectively (Ryer, 1998).

RESULTS

Transilluminated recordings

Our first experiments used point stimulation to compare the epi-illuminated and transilluminated voltage-dependent sig-

nal. Fig. 2 A is a view of the endocardial surface of a right ventricular slab preparation stained with the voltage-sensitive dye in epi-illumination mode. Details of the tissue surface are visible as small variations in brightness. Fig. 2 B shows the same preparation viewed from the same camera illuminated by the light behind the tissue. This is an image of fluoresced light escaping from inside the tissue. The lighter areas left of center correspond to small depressions in the endocardial surface, with the tissue being slightly thinner in these areas. To see an image with transillumination, the camera's black level was decreased to its lowest setting, and the gain increased until voltage-dependent changes in fluorescence were detectable. The emitted fluorescence collected at the camera lens (0.23 W/m^2) was nearly four orders of magnitude smaller than the level of excitation light at the tissue surface (740 W/m^2).

Fig. 2, C and D show unfiltered optical action potentials recorded from the same pixel during epi- and transillumination (*asterisks* in panels A and B). The vertical axis measures changes in fluorescence (in gray levels). Due to decreased light levels and lower signal intensity, the transillumination signals were significantly noisier. The average signal-to-noise ratios (SNR) at 240 fps were 7.7 ± 2.6 for epi-illuminated recordings and 2.0 ± 1.4 for transilluminated recordings ($n = 10$). Panels E and F show the same recordings after filtering (see Methods).

Isochrone maps of transmural propagation

Transilluminated recordings (the TRANS1 and TRANS2 movies) were used to construct isochronal maps for comparison with isochronal maps of endocardial and epicardial activation. Fig. 3 shows an example of such maps obtained when the preparation was paced from the endocardial surface at BCL = 500 ms. Panels A and D show the endocardial and epicardial maps obtained in standard epi-illumination mode. The endocardial sequence of activation (panel A) shows elliptical waves spreading from the tip of the electrode. The red 12-ms isochrone at the center shows the earliest activation times. The epicardial activation pattern on the opposite side of the slab (panel D) shows two breakthrough areas (green 20 ms isochrones) at the center and upper left. The widely spaced isochrones indicate rapid propagation, which would be expected from transmural breakthroughs. Panels B and C show isochronal maps constructed from transillumination data: TRANS1 was obtained with the epicardial camera and endocardial light source, TRANS2 with the endocardial camera and epicardial light source. The activation patterns in TRANS1 and TRANS2 maps are consistent with the surface recordings, showing breakthrough regions in the vicinity of the stimulating electrode. In addition, the conduction delays in these regions are intermediate between those on the surfaces, also consistent with endocardial-to-epicardial transmural propagation.

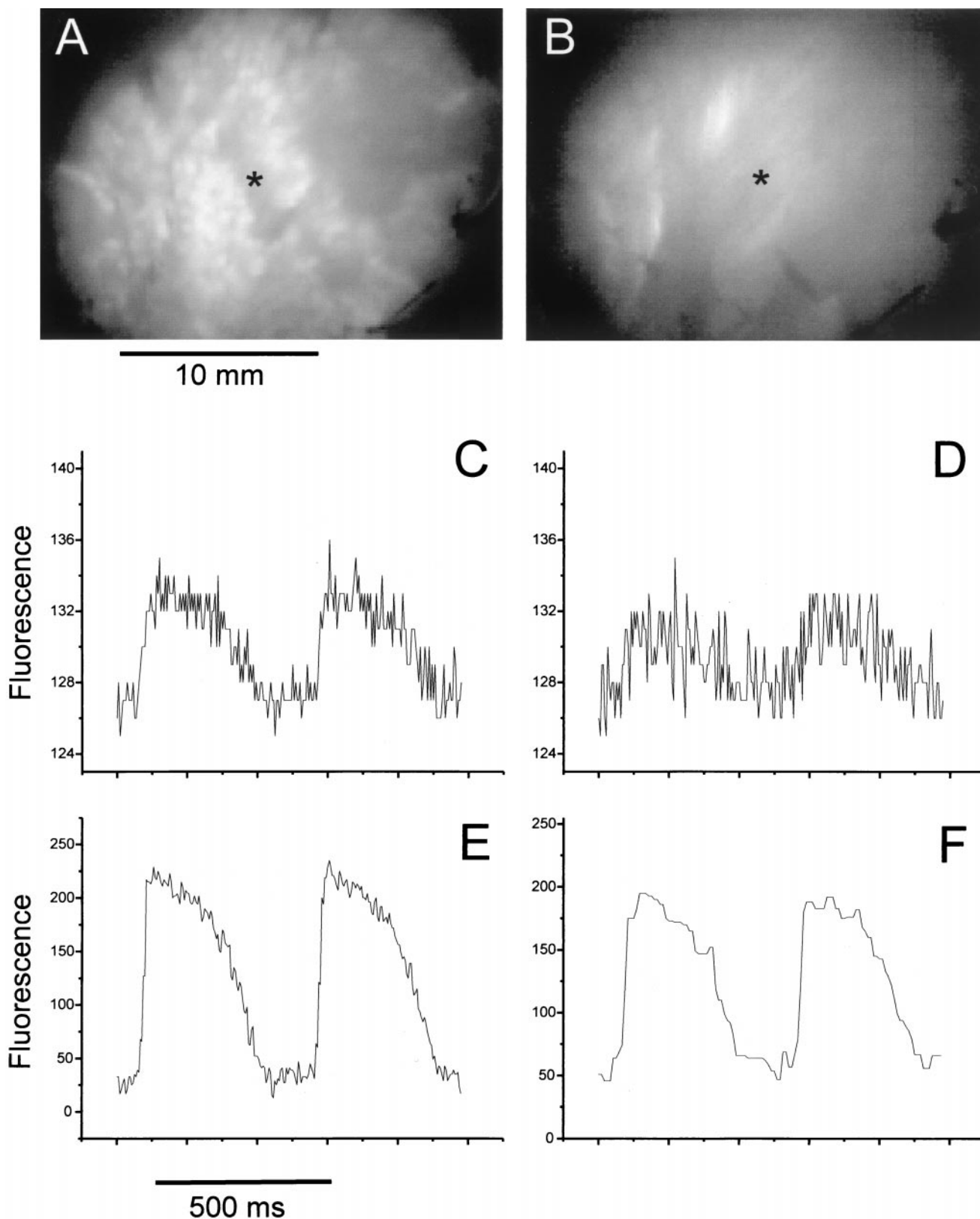


FIGURE 2 (A) Epi-illuminated view of sheep right ventricular slab. (B) Transilluminated view of same preparation. (C) Optical recording: values over time during epi-illumination from pixel marked with an asterisk in A. $S/N_{\text{RMS}} = 7.5$. Fluorescence units are gray levels. Time scale at bottom applies to panels C-F. (D) Optical recording from same point (asterisk in B) during transillumination. $S/N_{\text{RMS}} = 2.5$. (E) Recording from C after spatial filtering (kernel width = 11 pixels). (F) Recording from D after spatial filtering (kernel width = 15 pixels) and temporal median filtering (length = 9 frames).

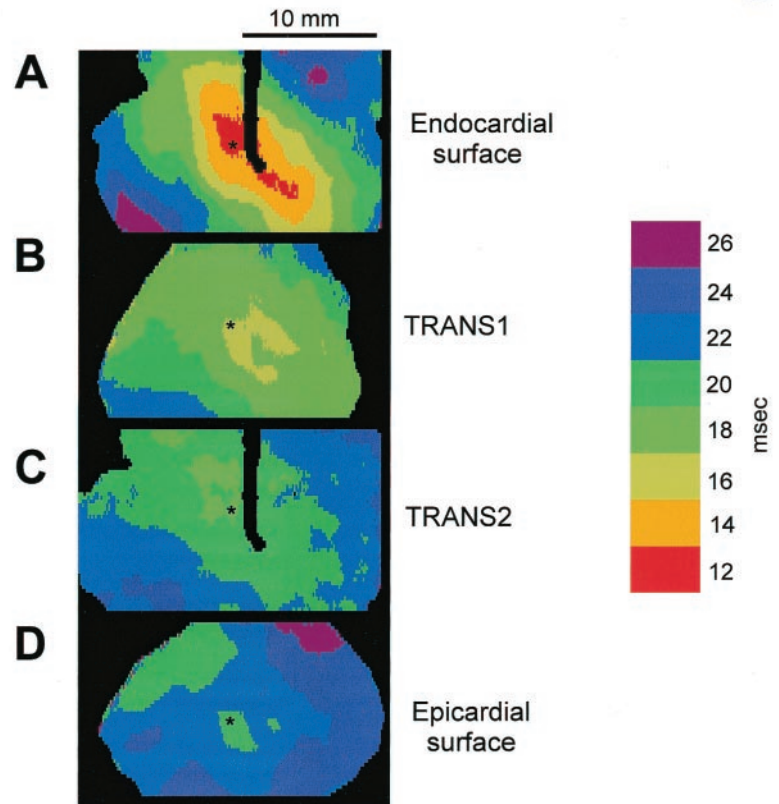
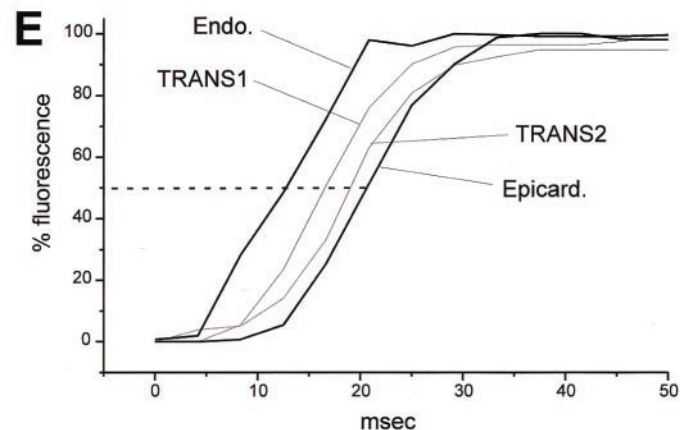


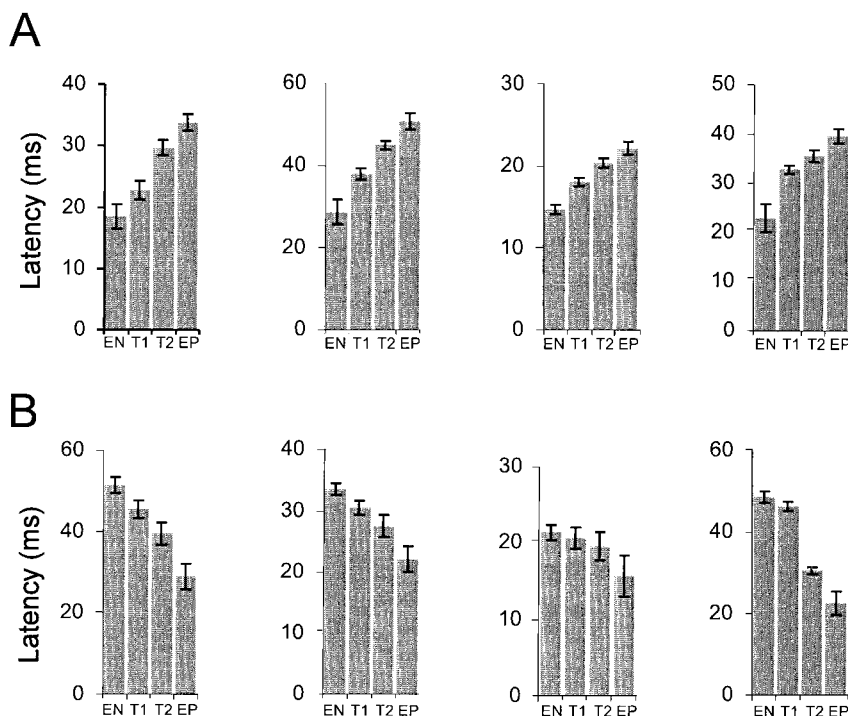
FIGURE 3 Isochronal maps of propagation resulting from stimulation on the endocardial surface. Isochrones are 2 ms apart, with red earliest and purple latest. (A) Endocardial surface map. Stimulating electrode appears as large black line in center. (B) Map of transilluminated movie with endocardial light source. (C) Map of transilluminated movie with epicardial light source. (D) Epicardial surface map showing breakthroughs. Views from the endocardial camera (A, C) have been flipped left to right to align them with the epicardial camera's viewpoint. (E) Optical activations from same x, y point (asterisks in A–D). Each has been normalized to 100%, and the activation time determined from the 50% level of the upstroke (dotted line).



Interestingly, TRANS1 and TRANS2 are not the same: the activation latencies in TRANS1 are, in general, smaller than in TRANS2. Fig. 3 E contains four optical action potentials recorded at the same point in x, y space from each of the four movies (asterisks in panels A–D), showing the progressively increasing delays. This order of activation in the area under the stimulating electrode was observed in all four transmural pacing experiments. Moreover, reversing the direction of transmural propagation by moving the stimulating electrode from the endocardium to the epicardium always resulted in the reversal of the activation delays in TRANS1 and TRANS2.

Fig. 4 shows average activation times from all four movies in a $5 \times 5 \text{ mm}^2$ area under the stimulating electrode for endocardial (top row) and epicardial (bottom row) stimulation. Although the activation delays varied in different experiments, in every tissue preparation ($n = 4$) the sequence of activation was always preserved: endo- < TRANS1 < TRANS2 < epi- during endocardial stimulation and epi- < TRANS2 < TRANS1 < endo during epicardial stimulation. The average latencies of the four transmural pacing experiments were (in ms): endocardial (21.2 ± 6.0), TRANS1 (27.9 ± 9.1), TRANS2 (32.7 ± 10.3), epicardial (36.6 ± 11.9) for endocardial stimulation, and epicardial

FIGURE 4 Transmural pacing: average latencies (time after stimulation) in 5×5 mm square region under the stimulating electrode in four different ventricular slabs. EN = endocardial movie, T1 = TRANS1, T2 = TRANS2, EP = epicardial movie. Top row shows endocardial stimulation, bottom row shows epicardial stimulation.



(22.3 ± 5.4), TRANS2 (29.3 ± 8.2), TRANS1 (35.7 ± 12.4), endocardial (38.7 ± 13.9) for epicardial stimulation.

We will show below that the observed differences in TRANS1 and TRANS2 can be fully explained based on the analysis of the contribution of different layers in the transillumination signal: the weighting function.

Light attenuation

The measurements of light attenuation in the tissue at the excitation and emission wavelengths were used to estimate the contribution of different layers to the transilluminated signal. Fig. 5 shows the cut transmural edge in one preparation, illuminated from the left at the emission (A) and excitation (B) wavelengths. The epicardial surface is on the left, the endocardial surface is on the right (in darkness). There was no fluorescent dye in the tissue. Panel C shows pixel values from a single horizontal row in each image. Both curves exhibit a slight increase in intensity within the first few hundred micrometers followed by an exponential decay; the reason for this subsurface peak will be discussed below. The subsurface peak is evident in D, in which the emission image (A) is displayed with a pseudocolor scale (brightest values in yellow and red). Each pixel row was shifted to vertically align the preparation edge, and its intensities stretched to the same maximum and minimum value (E). All selected rows were then averaged together, providing average excitation and emission profiles for each preparation (F). Exponential decay functions were fit to the profiles in F (for depths >1 mm). The penetration depth δ

(spatial decay constant) was significantly shorter for the excitation band of wavelengths ($\delta_{\text{ex}} = 0.77$ mm) than for the emission band ($\delta_{\text{f}} = 1.36$ mm). Table 1 shows the results of light attenuation measurements for preparations at different orientations of the slab with respect to the light source (see Methods). There were no significant differences in the penetration depths in the pairwise comparison of the transmural, epicardial, or endocardial groups ($p < 0.05$), indicating that the attenuation characteristics did not result from structural inhomogeneities, but from intrinsic optical characteristics of cardiac muscle.

A model of fluence rate

In order to derive the weighting functions, the profiles obtained with excitation light ($n = 12$) were averaged together to create an average profile for the penetration of excitation light, depicted by the thick line in Fig. 6 A. The same was done for the 12 profiles of red light, creating an average profile for the emission band (panel B). The excitation profile was fit with an expression for light intensity within a rectilinear slab irradiated by a uniform beam of collimated light (Gardner et al., 1996; Jacques, 1998):

$$\phi(z) = C_1 \exp(-k_1 z / \delta_{\text{ex}}) - C_2 \exp(-k_2 z / \delta_{\text{ex}}), \quad (1)$$

where $\phi(z)$ is the amount of light, or fluence rate, at depth z , and δ_{ex} is the penetration depth for the excitation light. The emission profile was fit with a simple exponential function,

$$G(z) = C_3 \exp(-k_3 z / \delta_{\text{f}}), \quad (2)$$

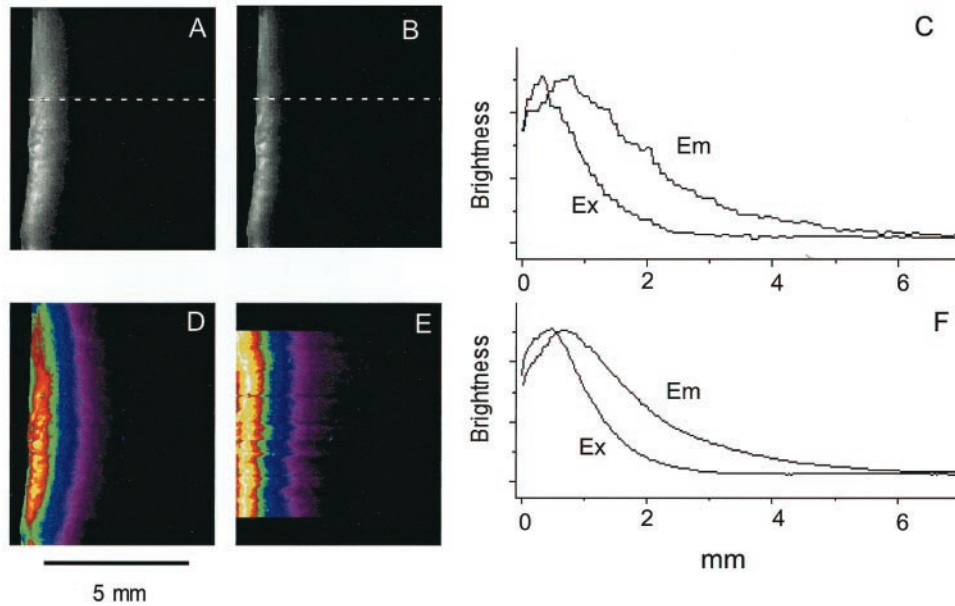


FIGURE 5 (A) View of transmural cross section of ventricular slab; the epicardium is on the left, endocardium is on the right. Emission wavelengths (590–690 nm) are incident from left side; view shows decay of light with tissue depth. Magnification = 0.025 mm/pixel. (B) Same tissue illuminated with excitation wavelengths (490–550 nm). (C) Pixel intensities from one horizontal row (*dotted lines* in A and B) show light decaying with depth for emission (Em) and excitation (Ex) wavelengths. (D) Same as (A) but with pseudocolor scale; brightest areas (*yellow/red*) are shifted slightly away from the illuminated surface. Each row was shifted to the left, then normalized by stretching all intensities to the same maximum and minimum (E). All rows were then averaged to create average profiles for both excitation and emission wavelengths (F).

where $G(z)$ is the escape of fluorescence from depth z and δ_f is the penetration depth for the emission wavelengths. Equation 1 has a second exponential term to account for photons “leaking” out of the tissue near the surface (see Discussion). This extra term is not included for the escape function G because the photons of interest are already exiting the medium. The parameters C_i and k_i were free variables used during the fitting process: k_1, k_3, C_3 were set to 1; the other values were $C_1 = 927, C_2 = 702, k_2 = 1.8$ (see Gardner et al., 1996). In Fig. 6 C, the solid lines show the fit of Eqs. 1 and 2, respectively, to the average excitation (*filled circles*), and emission (*open circles*) profiles.

The expressions for $\phi(z)$ and $G(z)$ were used to calculate the weighting functions $g_i(z)$, which characterize the contributions of internal layers to the total fluorescence escaping from either side of the slab. For epi-illumination (g_1), the amount of fluorescence emitted from depth z is the product of the fluence and escape expressions, normalized

by the denominator representing the total fluorescence emitted from the side being illuminated,

$$g_1(z) = \frac{\phi(z)G(z)}{\int_0^w \phi(z)G(z)dz} \quad (3)$$

where w is the total depth of the tissue and depth $z = 0$ is the illuminated surface. Then for transillumination (g_2), the amount of fluorescence emitted from depth z out the side opposite the light source is

$$g_2(z) = \frac{\phi(z)G(w-z)}{\int_0^w \phi(z)G(w-z)dz} \quad (4)$$

The remaining weighting functions, $g_3(z)$ and $g_4(z)$, are the mirror reflections of the first two with respect to the center of the preparation.

Fig. 7 shows the percent contribution from each 100 μm bin across an 8-mm-thick slab, for epi-illumination (*top*) and transillumination (*middle*) with light incident from the left. With epi-illumination, 82% of the total fluorescence is emitted from within the first millimeter beneath the irradiated surface. With transillumination, the same superficial region contributes only 30% of the total fluorescence, with the rest of the fluorescence coming from deeper layers (90% by 4 mm). The shape of the transillumination function offers

TABLE 1 Average penetration depths (δ) for ventricular slabs

	δ_{ex} (mm)	δ_f (mm)	N
Transmural edge	0.85 ± 0.22	1.31 ± 0.24	6
Epicardium	0.71 ± 0.05	1.33 ± 0.20	3
Endocardium	0.82 ± 0.10	1.42 ± 0.17	3
Mean	0.80 ± 0.16	1.34 ± 0.20	12

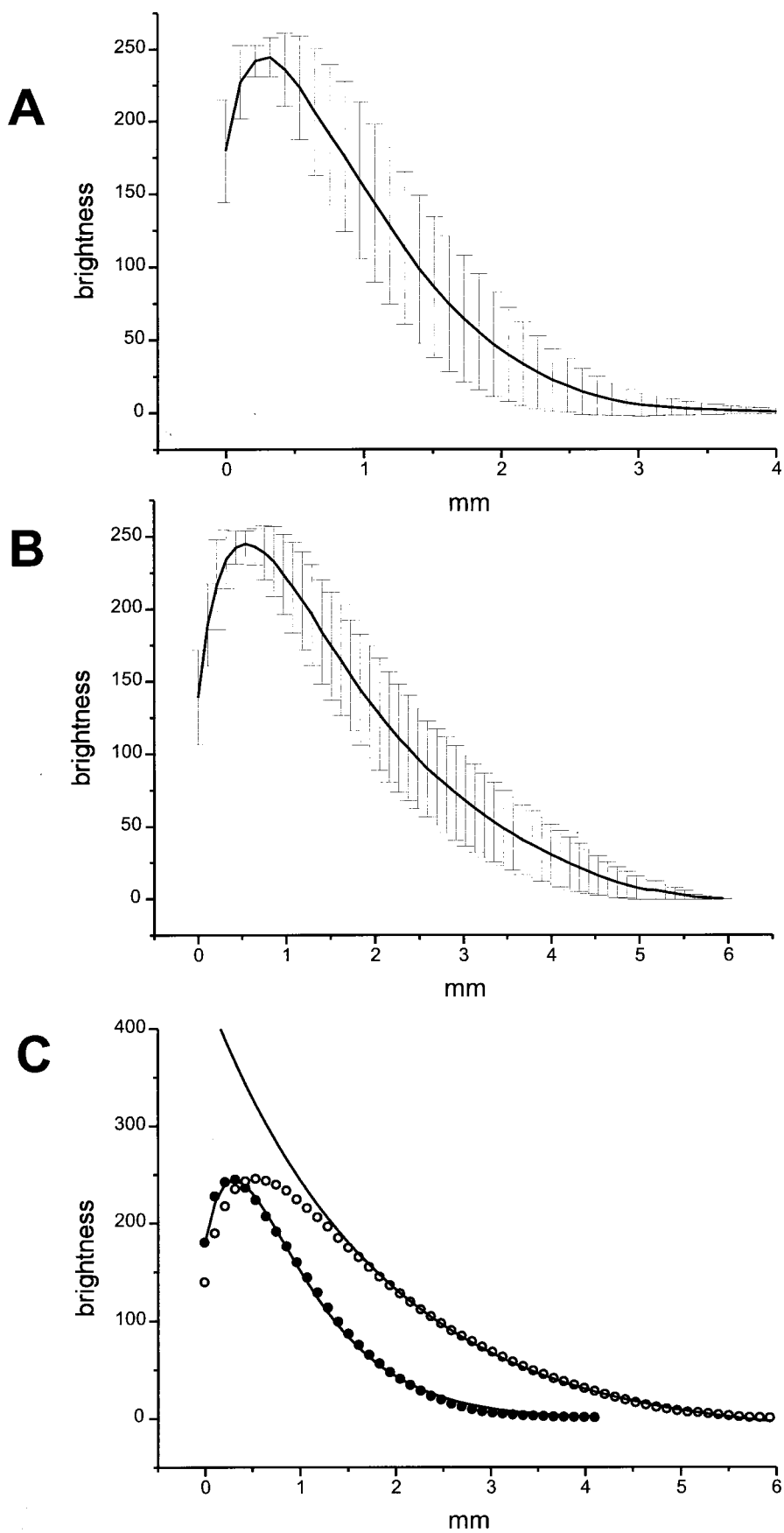


FIGURE 6 Average of 12 profiles of (A) green excitation light and (B) red emission light. Note differences in horizontal scales. Error bars show standard deviations. (C) The average excitation (filled circles) and emission profiles (open circles) and the fit with Eqs. 1 and 2, respectively (solid lines, see text).

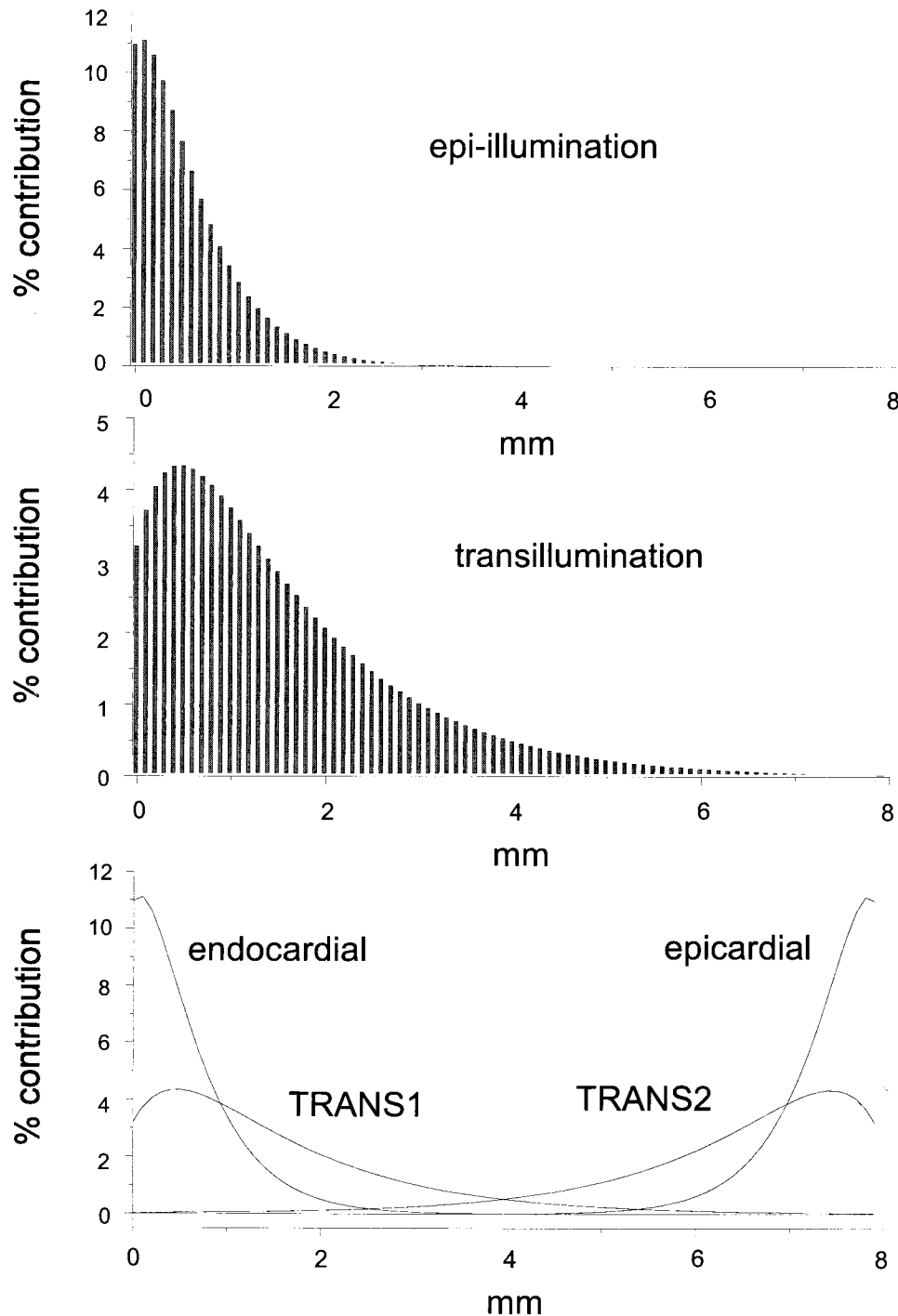


FIGURE 7 (Top) The calculated percent contribution of each layer (in 100 μm bins) to the total epi-illuminated signal in an 8-mm-thick slab of tissue. (Light is incident on the left side, light is collected from left side of slab.) (Middle) The percent contribution of each 100 μm bin to the total transilluminated signal (excitation light incident on left side, emitted light collected from right side). (Bottom) Distributions showing contribution to total signal in endocardial, TRANS1, TRANS2, and epicardial movies. Light is from the left for endocardial and TRANS1, from the right for TRANS2 and epicardial.

a qualitative explanation for the ordering of the isochrone maps in Fig. 3 and the activation times in Fig. 4. The majority of the signal recorded via transillumination ema-

nates from layers under the illuminated surface, but they are a weighted sum of these deep layers, in which the most superficial layers make only a minor contribution. Fig. 7,

bottom shows the endocardial (g_1) and TRANS1 (g_2) weighting functions for light incident from the left, and the TRANS2 (g_3) and epicardial (g_4) weighting functions for light incident from the right. These show the percent of light from each layer in an 8-mm slab of tissue contributing to each of the four movies in the optical recording protocol described in Fig. 1.

Simulation of optical signals during transmural propagation

With the weighting functions in hand, it was possible to optically estimate recorded action potentials in epifluorescence and transillumination modes. Optical recordings $H_1(t)$ were simulated using a digitized action potential from a microelectrode recording of sheep ventricular muscle (Fig. 8 A, *inset*). For each point in time, the product of the electrical signal times the contribution of light was summed over all positions:

$$H_1(t) = \int g_i(z)a(ct - z)dz$$

where a was the spatial profile of the action potential, c was the transmural propagation velocity, and g_i was one of the four weighting functions in Fig. 7, *bottom*. The solid lines in Fig. 8 A show the calculated upstrokes of the four optical recordings: (a) endocardial movie, (b) TRANS1, (c) TRANS2, and (d) epicardial movie. There is evident qualitative similarity between these simulated recordings and the optical recordings in Fig. 3 E. The simulated transilluminated recordings have slow upstrokes, the result of being smeared by summation of multiple layers. The surface recordings are less smeared, since only 1–2 mm of tissue contribute to them. Notably, the model exhibits the difference between TRANS1 and TRANS2 described above. Indeed, the sequence of activation was the same as in the experiment (endo- < TRANS1 < TRANS2 < epi). However, the difference between activation times in TRANS1 and TRANS2 was much larger in computer simulations than in the slab preparations. Differences in relative latencies may be attributable to variations in transmural propagation velocity in the tissue, versus uniform velocity in the simulation. The optical upstrokes in Fig. 3 E are also more uniform than the simulations: this may result from the limited temporal resolution of the video camera system.

In our preparations, the attenuation of light with depth did not follow simple exponential decay, but instead exhibited a decrease near the illuminated face, resulting in a peak of intensity just below the surface (Figs. 5 and 6). How does the subsurface maximum of fluence affect the transilluminated signal? The second term in Eq. 1 represents scattering losses from the surface, producing the boundary effect. If this term is dropped, the model becomes one of simple

exponential decay for both excitation and emission wavelengths (see Girouard et al., 1996). The percent contribution from each layer was recomputed in this simple model, resulting in the weighting functions for the endocardial and TRANS1 movies in Fig. 8 B (*dotted lines*). Compared to the corresponding weighting functions from Fig. 7, *bottom* (*solid lines*), the simple model predicts only exponential decay, with the greatest contributions coming from layers at the illuminated surface. Optical recordings were simulated with all four weighting functions from the simple model, shown as dotted traces in Fig. 8 A. The transilluminated traces b and c are shifted toward their respective surface traces a and d if there are no scattering losses from the surface. While this does not dramatically alter the interpretation of the maps, it indicates that the subsurface rise due to scattering does move the apparent source deeper into the tissue.

The model was also used to test the effects of varying the thickness of the preparation. Transillumination weighting functions were generated for slabs ranging from 2 to 10 mm (Fig. 8 C). For tissues thicker than 6 mm, the contributions remain essentially unchanged, since the amount of fluorescence beyond 6 mm depth is negligible. For a 4 mm slab, the decaying tail is truncated, slightly increasing the percent contribution of the remaining layers. This effect is exaggerated at 2 mm, with the peak contribution at 0.5 mm (see Discussion).

Using transillumination for detection of intramural reentrant activity

Transillumination can provide useful information about three-dimensional propagation in the thickness of the myocardial wall during ventricular arrhythmias. Fig. 9 depicts an example of sustained monomorphic ventricular tachycardia in which transillumination reveals intramural reentrant activity (intramural scroll wave) that otherwise could not be detected from only epifluorescence recordings. Panel A shows epicardial, subepicardial (TRANS2), subendocardial (TRANS1), and endocardial isochronal maps constructed from the epi-illumination and transillumination recordings. Both surfaces exhibited breakthrough patterns of activity without identifiable reentry patterns. Indeed, the endocardial surface map contains a breakthrough (*green*), but no rotating activity. However, the simultaneously recorded subendocardial map has rotating activity around a small core near the center. In addition, there is clockwise rotating propagation in the upper right corner that does not form a complete circuit. A region of extremely slow propagation (*yellow*) lies between these two circuits, creating a pattern greatly resembling figure-of-8 reentry (El-Sherif et al., 1981).

Similar results were obtained using epicardial illumination. The epicardial surface map shows a breakthrough of activity (*red*) in the upper right region. Although areas of slow propagation (crowding of isochrones) can be identified, no reentrant activity can be seen on the surface. The

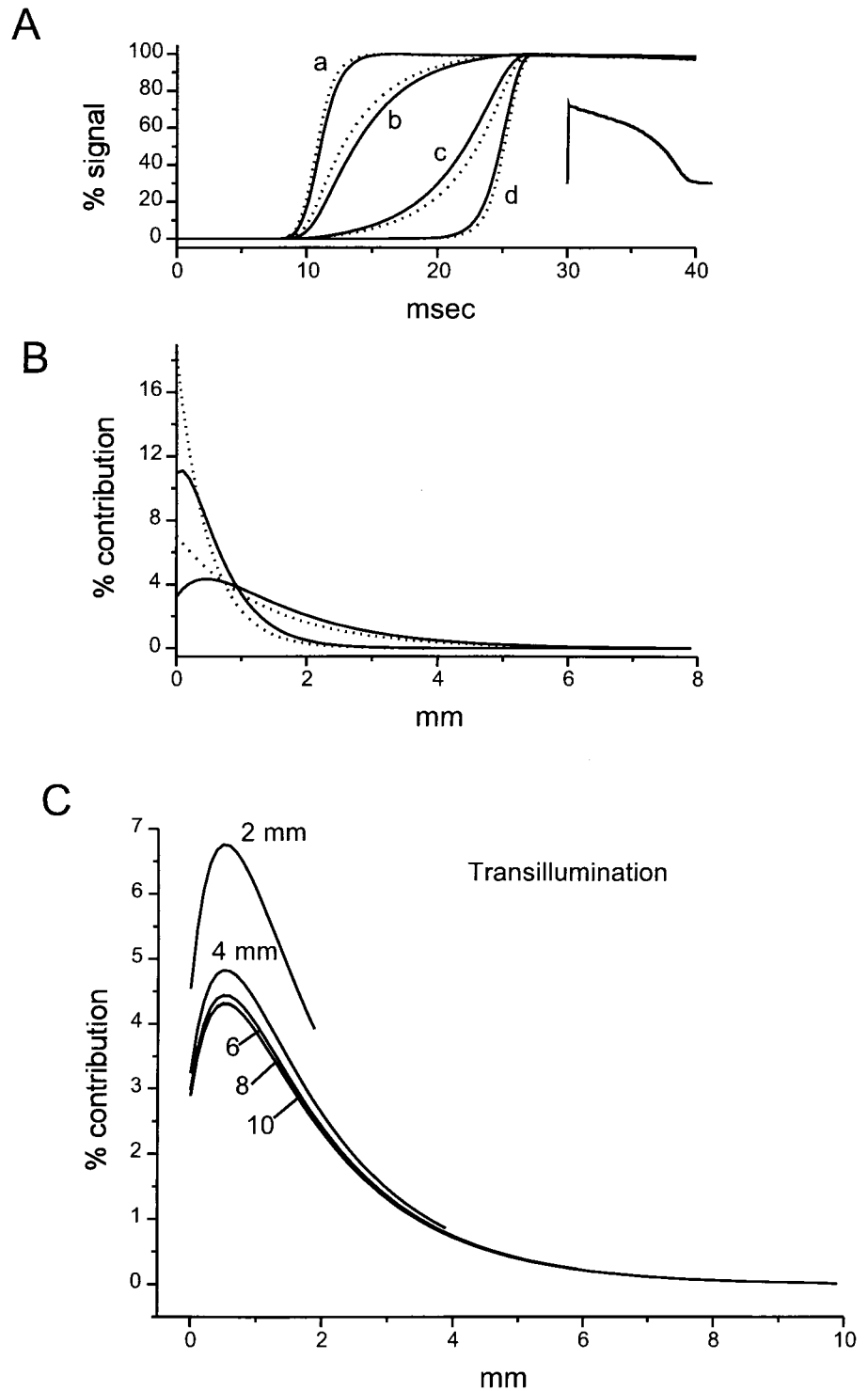


FIGURE 8 (A) Solid lines: four simulated optical recordings obtained by convolution of an action potential (*inset*) with each of the four weighting functions in Fig. 7, *bottom*. (a) Endocardial camera with epi-illumination, (b) epicardial camera with transillumination (TRANS1), (c) endocardial camera with transillumination (TRANS2), (d) epicardial camera with epi-illumination. The action potential was digitized from a microelectrode recording from sheep ventricular muscle. *Dotted lines*: simulated optical recordings from a model of simple exponential decay for excitation wavelengths (see text). (B) *Solid line*: plots showing contribution from different layers (same as endocardial and TRANS1 in Fig. 7, *bottom*). *Dotted line*: same plots for model without scattering losses at border. (C) The percent contribution to transilluminated fluorescence computed across the ventricular slab for several slab thicknesses (in mm).

simultaneously recorded subepicardial map contains a large linear “breakthrough” area (*red*) directly under the epicardial breakthrough, but this is part of a complete reentrant circuit, rotating counterclockwise around a small circular core (*black*).

A hypothetical filament (elongated center of rotation; see Winfree, 1973; Pertsov and Jalife, 1995) of the scroll wave that fulfills all these constraints is shown in Fig. 9 *B*. The filament starts near the epicardial surface on the left lateral edge of the slab, crosses two transillumination layers, bends

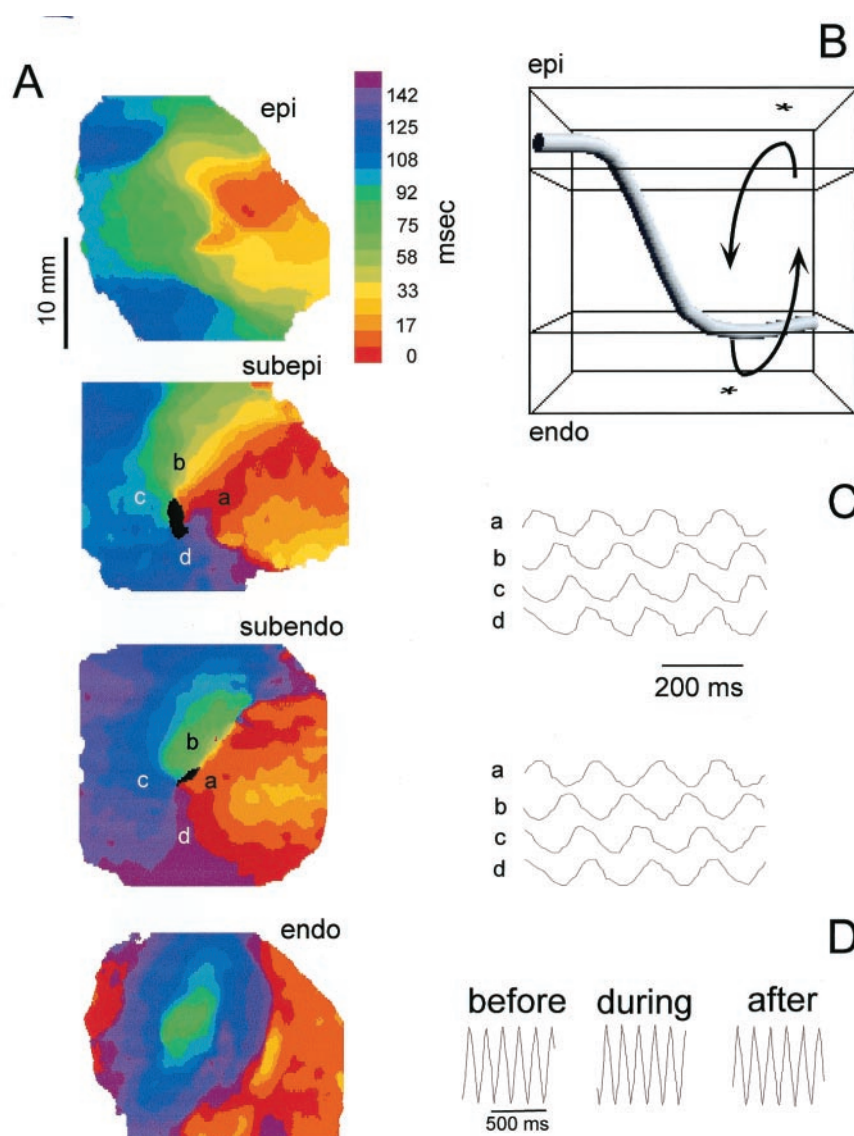


FIGURE 9 (A) Intramural reentry: 8.3 ms isochrones of monomorphic VT that exhibited breakthroughs in the surface recordings (red isochrones in epicardial map, green in endocardial map), and counterclockwise rotation in the transilluminated recordings (subepi- and subendocardial maps). The filament was probably aligned along the line of slow propagation (yellow isochrone in subendocardial map). (B) Putative intramural filament with transmural rotation (*arrows*) resulting in surface breakthroughs (*asterisks*). (C) Optical recordings from single points around the reentrant circuits in the subepicardial (*upper traces*) and subendocardial (*lower traces*) maps. (D) Pseudo-ECGs of endocardial optical recordings indicate stability of activity before, during, and after transillumination recordings.

back up toward the subendocardial plane, and ends at the right lateral edge. Rotation of activity causes the wave front to travel in an epicardial-to-endocardial path, and then reverse direction (*arrows*), resulting in breakthroughs on the two surfaces (*asterisks*) that are out of phase in time and offset in space (compare epi- and endocardial maps).

Fig. 9 C shows optical recordings around the reentrant circuits in the transilluminated movies (upper traces from subepicardial, lower traces from subendocardial). Panel D contains the pseudo-ECGs (Pertsov et al., 1993; Davidenko, 1993) of the endocardial surface movies acquired before (both lights), during (endocardial light), and after (both lights) the transilluminated recordings to demonstrate the stability of the excitation pattern. Similarly, the activations on the electronic ECG were stable and maintained the 150 ms cycle length during the 4 min required to obtain the complete series of control and transilluminated recordings (data not shown).

DISCUSSION

The overall aim of this project was to test the feasibility of extending the optical mapping technique to record fluorescence from deep layers of cardiac tissue. We present here the first systematic demonstration that transilluminated fluorescence may be used to detect electrical activity within cardiac muscle. Compared to epi-fluorescence, much less light is transmitted through the tissue, greatly reducing the SNR of the transilluminated voltage-dependent signal. Nevertheless, identifiable activations were obtained after filtering. Isochronal maps of waves propagating transmurally in the ventricle showed that the transilluminated movies contained information distinguishable from the surface movies, and that they more closely resembled the activity on the surface nearer the light source. The non-uniform contributions of different layers to transillumination signal is a result of higher attenuation of the excitation light as compared to fluorescence inside the tissue.

Earlier experiments in our laboratory attempted to precisely localize the depth of the transilluminated signal, using intramural electrodes and epifluorescence data from the cut transmural edge. Those results showed that the 50% level of the transilluminated optical activations corresponded to the point in time when the wave front was located ~ 2 mm beneath the illuminated surface (Baxter et al., 1997a, 1999). However, measurements of light penetration and the model of escaping fluorescence indicated that the transilluminated signal is the weighted sum of contributions from the entire width of the ventricle, illustrated by the weighting functions of Fig. 7. Computer simulations incorporating these weighting functions in an 8-mm slab confirmed that the midpoint of the smeared transilluminated upstroke consistently corresponded to the moment when the wave front was 1.5–3 mm beneath the surface, for a variety of different propagation patterns, including a simulated intramural scroll wave (Baxter, 1999). Therefore, although it is the summation of light from several millimeters of tissue, the transilluminated signal gives the appearance of originating from a fairly restricted depth. One way to explain this phenomenon is that the weighting function of Fig. 7, *middle* has a center of mass at 1.8 mm; as the transilluminated recording accumulates, the wavefront passes through this center at the midpoint of the temporal recording. In this article we have not attempted to assign the TRANS1 and TRANS2 movies to a particular depth, but rather to stress the activation order relative to the surface movies, and how this creates a consistent picture of three-dimensional propagation in the ventricle.

The transilluminated signal

Our data are consistent with observations that biological tissues exhibit spectral sensitivity: longer wavelengths have a higher transmittance, i.e., are able to penetrate more deeply, while shorter wavelengths are quickly attenuated (Preuss et al., 1983; Wilson et al., 1985; Girouard et al., 1996). This results in the distribution of layers contributing to the transilluminated signal in Fig. 7, *middle*: the short excitation light is unable to penetrate very deeply, but once a fluorophore is excited, the longer-wavelength fluoresced light is able to escape from the tissue.

The optical penetration depth δ characterizes the $1/e$ attenuation of light in tissue for a given wavelength (Wilson et al., 1985; Cheong et al., 1990; Jacques, 1998). Measurements of δ in muscle at the wavelengths considered here show considerable variation in the literature. Wilson et al. (1985), positioning optical fibers at different depths in rabbit skeletal muscle, calculated penetration depths around 2 and 3 mm for 514 and 630 nm light, respectively. Girouard et al. (1996) used transmission spectra of guinea pig ventricle to calculate decay constants of 0.289 and 0.434 mm for 540 and 640 nm wavelengths, respectively. The properties of light transport through tissue vary considerably

depending on the wavelength, the type of tissue, and the geometry of the preparation and irradiation (Cheong et al., 1990). Variations in experimental technique and tissue preparation also add to differences in reported values. We directly measured the attenuation of light using the same tissue preparations, wavelength bands, and photodetectors used in our optical mapping experiments. Our measured decay constants (0.8 and 1.3 mm for excitation and emission) fall within the range of previously published values.

Our preparations exhibited a pronounced boundary effect in the profiles of light attenuation in the form of a peak beneath the surface (Figs. 5 and 6). This subsurface peak of light distribution in highly scattering media with slab geometry has been observed in analytical solutions to the light transport equation (Star et al., 1988), simulations based on diffusion theory (Profio and Doiron, 1987; Flock et al., 1989), and Monte Carlo models (Gardner et al., 1996; Jacques, 1998), as well as empirically in phantoms and muscle tissue (Marynissen and Star, 1984; Gardner et al., 1996). It has been explained as resulting from the loss of scattered photons from tissue near the surface (Svaasand, 1984; Profio and Doiron, 1987). The subsurface maximum in the light penetration profiles (Fig. 5) in turn causes the weighting functions to have subsurface maxima as well (Fig. 7). In contrast, a fluence model with simple exponential decay in both the excitation and emission wavelengths has contributions that decrease monotonically from the illuminated surface (Fig. 8 *B*). The subsurface peak does have the effect of moving the apparent source of the transilluminated signal deeper into the tissue. However, the primary reason that the TRANS movies in our preparations have activation times and isochronal patterns intermediate between those of the surface movies is that the bulk of the transilluminated signal originates from the first 3–4 mm of tissue under the illuminated surface.

The epi-illuminated signal

According to our estimates, during epi-illumination, layers as deep as 2 mm beneath the surface may contribute to the signal (Fig. 7, *top*). This value is significantly larger than previous estimates that only a thin (0.3–0.5 mm) layer of cells at the surface contributes to the measured fluorescence. Using a wedge of rabbit ventricle perfused with di-4-ANEPPS, Knisley (1995) found that fluorescence increased with increasing thickness of the wedge, up to ~ 300 μm , suggesting that dye in deeper layers was not contributing fluorescence. Girouard et al. (1996) calculated excitation and emission decay constants by measuring transmission spectra for perfused di-4-ANEPPS in guinea pig ventricle, and estimated that 95% of the signal detected from the surface emanates from a depth < 500 μm . There are several possible reasons for this discrepancy. Change in the penetration depths would affect the distributions in Fig. 7, *top* and *middle*, by stretching or compressing the graphs along

the horizontal axis. Smaller δ values would predict that epi-illumination results from only the most superficial layers; larger δ values would predict that even deeper layers contribute to the epi-fluorescent signal. Given the variation of these values in the literature (Cheong et al., 1990), the penetration depths we measured are probably the best estimates for our experimental setup, and their resulting estimates of light distribution are consistent with our observations (simulated versus optical action potentials). Another factor may be the depth of field of the recording system, in that the unfocused fluorescence from deeper layers may have a reduced contribution. Our optical system had a significantly larger depth of field than the system used by Girouard et al. (>8 mm vs. 50–200 μm) and most other systems incorporating photodiodes (Salama et al., 1994; Knisley, 1995). Nevertheless, it should be noted that unfocused light still adds to the total collected fluorescence. Illumination geometry also affects the amount of excited tissue: a thin laser beam (Knisley, 1995) may result in a more rapid decrease in excitation fluence than a broad beam of uniform illumination. Penetration depth could also be affected by the presence of dye, which would presumably increase absorption and therefore produce more rapid attenuation (Baxter, in press). However, our measurements of penetration depth in dye-perfused tissue (data not shown) were not different from the results presented above.

Finally, it should be noted that some optical recordings may be summing signals from deeper layers than previously realized. The presence of dual-humped activations in surface recordings during ventricular tachycardia in the rabbit heart led Efimov et al. (2000) to conclude they were observing scroll waves with the filaments parallel to the surface, 1–2 mm deep.

Limitations

In the approach described here, acquisition of all four sets of data (endocardial, TRANS1, TRANS2, epicardial), required two trials, thus limiting the usefulness of the technique to the study of repetitive phenomena such as pacing and monomorphic tachycardia. Nonrepetitive phenomena, such as the irregular patterns of tachycardia and fibrillation, are restricted only to “single-sided” recordings. (The experimental protocol allows simultaneous acquisition of epi-illuminated and transilluminated data, using two cameras and one light). This limitation might be overcome, for example, by using an optical chopper synchronized to the cameras’ frame intervals, to rapidly deliver light to opposite sides of the preparation.

It should be noted that isochronal maps constructed from transillumination data have a significantly lower resolution than surface maps, both laterally and in the depth of the tissue. The transillumination signal integrates fluorescence from a much thicker layer than epi-illumination, resulting in approximately a threefold reduction in depth resolution (3

mm vs. 1 mm). This must be kept in mind even if the transilluminated data can be roughly treated as a subsurface layer (see above). Lateral light-scattering decreases spatial resolution in the usual sense of localization in the image plane. The model of light transport we have used represents excited fluorophores as isotropic point sources of emission photons (Gardner et al., 1996). Fluorescent light is scattered in all directions, laterally within the myocardium as well as toward the photodetector. This will induce significant blurring during image formation, with deeper layers having greater blurring. The wavefronts in our transilluminated movies of voltage-dependent activity did appear slightly blurred in space when compared to our epi-illuminated recordings, but the differences were not objectionable. For transillumination to become a more precise tool, an important future step would be the quantification of scatter-induced blurring versus depth and its inclusion into the model.

Interpretation of the transillumination signal is also affected by the width of the preparation. In thicker tissues (>6 mm), the weighting functions change very little, indicating that the transilluminated signal will still integrate about the same amount of tissue under the irradiated surface (Fig. 8 C). However, as thickness increases, total emitted fluorescence and signal strength decrease, while the amount of spatial blurring induced by lateral scattering increases. Therefore, although the contributing layers under the illuminated surface remain fairly constant with increasing thickness, the resulting signal will be deteriorated by low SNR and blurring. These problems are reduced in thinner preparations. However, as the slabs are thinned to 2 mm, all of the weighting functions will have significant overlap, making it difficult to distinguish the two transilluminated movies from each other, and from the epi-illuminated signals.

In conclusion, the present work represents the first quantitative step in understanding the transillumination signal and its use in studies of three-dimensional wave propagation in the heart. Optical mapping combining both epi-illumination and transillumination shows promise as a technique for elucidating the complex waveforms that underlie many cardiac arrhythmias.

REFERENCES

- Baxter, W. T. 1999. Intramural Optical Recordings of Cardiac Electrical Activity via Transillumination. Ph.D dissertation. Department of Pharmacology, SUNY Health Science Center, Syracuse, NY.
- Baxter, W. T. Optical properties of cardiac tissue. 2001. In *Optical Mapping of Cardiac Excitation and Arrhythmias*. D. S. Rosenbaum and J. Jalife, editors. Futura Publishing. (in press)
- Baxter, W. T., J. M. Davidenko, L. M. Loew, J. P. Wuskell, and J. Jalife. 1997b. Technical features of a CCD video camera system to record cardiac fluorescence data. *Ann. Biomed. Eng.* 25:713–725.
- Baxter, W. T., A. M. Pertsov, O. Berenfeld, S. F. Mironov, and J. Jalife. 1997a. Demonstration of three-dimensional reentry in isolated sheep right ventricle. *Pacing and Clinical Electrophysiology*. 20:1080.

- Cheong, W. F., S. A. Prael, and A. J. Welch. 1990. A review of the optical properties of biological tissues. *IEEE J. Quant. Electron.* 26:2166–2185.
- Davidenko, J. M. 1993. Spiral wave activity: a possible common mechanism for polymorphic and monomorphic ventricular tachycardias. *J. Cardiovasc. Electrophysiol.* 4:730–746.
- Dillon, S. M., T. E. Kerner, J. Hoffman, V. Menz, K. S. Li, and J. J. Michele. 1998. A system for in vivo cardiac optical mapping. *IEEE Eng. Med. Biol. Mag.* 17:95–108.
- Efimov, I. R., V. Sidorov, Y. Cheng, and B. Wollenzier. 2000. Evidence of three-dimensional scroll waves with ribbon-shaped filament as a mechanism of ventricular tachycardia in the isolated rabbit heart. *J. Cardiovasc. Electrophysiol.* 10:1452–1462.
- El-Sherif, N., M. Chinushi, E. B. Caref, and M. Restivo. 1997. Electrophysiological mechanism of the characteristic electrocardiographic morphology of torsade de pointes tachyarrhythmias in the long-QT syndrome: detailed analysis of ventricular tridimensional activation patterns. *Circulation.* 96:4392–4399.
- El-Sherif, N., R. A. Smith, and K. Evans. 1981. Canine ventricular arrhythmias in the late myocardial infarction period. 8. Epicardial mapping of reentrant circuits. *Circ. Res.* 49:255–265.
- Fast, V. G., and A. G. Kleber. 1993. Microscopic conduction in cultured strands of neonatal rat heart cells measured with voltage-sensitive dyes. *Circ. Res.* 73:914–925.
- Flock, S. T., M. S. Patterson, B. C. Wilson, and D. R. Wyman. 1989. Monte Carlo modeling of light propagation in highly scattering tissue. I. Model predictions and comparison with diffusion theory. *IEEE Trans. Biomed. Eng.* 36:1162–1168.
- Frazier, D. W., P. D. Wolf, J. M. Wharton, A. S. Tang, W. M. Smith, and R. E. Ideker. 1989. Stimulus-induced critical point. Mechanism for electrical initiation of reentry in normal canine myocardium. *J. Clin. Invest.* 83:1039–1052.
- Gardner, C. M., S. L. Jacques, and A. J. Welch. 1996. Light transport in tissue: accurate expressions for one-dimensional fluence rate and escape function based upon Monte Carlo simulation. *Lasers in Surgery and Medicine.* 18:129–138.
- Girouard, S. D., K. R. Laurita, and D. S. Rosenbaum. 1996. Unique properties of cardiac action potentials recorded with voltage-sensitive dyes. *J. Cardiovasc. Electrophysiol.* 7:1024–1038.
- Jacques, S. L. 1998. Light distributions from point, line and plane sources for photochemical reactions and fluorescence in turbid biological tissues. *Photochem. Photobiol.* 67:23–32.
- Knisley, S. B. 1995. Transmembrane voltage changes during unipolar stimulation of rabbit ventricle. *Circ. Res.* 77:1229–1239.
- Marynissen, J. P. A., and W. M. Star. 1984. Phantom measurements for light dosimetry using isotropic and small aperture detectors. *Progr. Clin. Biol. Res.* 170:133–148.
- Pertsov, A. M., W. T. Baxter, C. Cabo, R. A. Gray, J. M. Davidenko, and J. Jalife. 1994. Transillumination of the myocardial wall allows optical recording of 3-dimensional electrical activity. *Circulation.* 90:1-411.
- Pertsov, A. M., J. M. Davidenko, R. Salomonsz, W. T. Baxter, and Jalife. 1993. Spiral waves of excitation underlie reentrant activity in isolated cardiac muscle. *Circ. Res.* 72:631–650.
- Pertsov, A. M., and J. Jalife. 1995. Three-dimensional vortex-like reentry. In *Cardiac Electrophysiology*. D. P. Zipes and J. Jalife, editors. W. B. Saunders Co., Philadelphia. 403–410.
- Pogwizd, S. M., and P. B. Corr. 1987. Reentrant and nonreentrant mechanisms contribute to arrhythmogenesis during early myocardial ischemia: results using three-dimensional mapping. *Circ. Res.* 61:352–371.
- Preuss, L. E., F. P. Bolin, and B. W. Cain. 1983. A comment on spectral transmittance in mammalian skeletal muscle. *Photochem. Photobiol.* 37:113–116.
- Profio, A. E., and D. R. Doiron. 1987. Transport of light in tissue in photodynamic therapy. *Photochem. Photobiol.* 46:591–599.
- Rohr, S., and B. M. Salzberg. 1994. Multiple-site optical recording of transmembrane voltage (MSORTV) in patterned growth heart cell cultures: assessing electrical behavior, with microsecond resolution, on a cellular and subcellular scale. *Biophys. J.* 67:1301–1315.
- Ryer, A. D. 1998. *Light Measurement Handbook*. International Light, Inc., Newburyport, MA.
- Salama, G., A. Kanai, and I. R. Efimov. 1994. Subthreshold stimulation of Purkinje fibers interrupts ventricular tachycardia in intact hearts. Experimental study with voltage-sensitive dyes and imaging techniques. *Circ. Res.* 74:604–619.
- Salama, G., R. Lombardi, and J. Elson. 1987. Maps of optical action potentials and NADH fluorescence in intact working hearts. *Am. J. Physiol. Heart Circ. Physiol.* 252:H384–H394.
- Star, W. M., J. P. Marynissen, and M. J. van Gemert. 1988. Light dosimetry in optical phantoms and in tissues. I. Multiple flux and transport theory. *Physics in Medicine and Biology.* 33:437–454.
- Svaasand, L. O. 1984. Optical dosimetry for direct and interstitial photoradiation therapy of malignant tumors. *Progr. Clin. Biol. Res.* 170:91–114.
- Wikswa, J. P. J., S. F. Lin, and R. A. Abbas. 1995. Virtual electrodes in cardiac tissue: a common mechanism for anodal and cathodal stimulation. *Biophys. J.* 69:2195–2210.
- Wilson, B. C., W. P. Jeeves, and D. M. Lowe. 1985. In vivo and post mortem measurements of the attenuation spectra of light in mammalian tissues. *Photochem. Photobiol.* 42:153–162.
- Winfree, A. T. 1973. Scroll-shaped waves of chemical activity in three dimensions. *Science.* 181:937–939.
- Witkowski, F. X., L. J. Leon, P. A. Penkoske, W. R. Giles, M. L. Spano, W. L. Ditto, and A. T. Winfree. 1998. Spatiotemporal evolution of ventricular fibrillation. *Nature.* 392:78–82.